Original Research Article

Synthesis, Spectral Characterization, DNA Binding, Cleavage and Biological Evaluation on Co(II), Ni(II) and Cu(II) Complexes of Substituted Isoxazole Schiff Bases

Abstract

A series of $Co(L^{I})_2$ (**1**), $Ni(L^{I})_2$ (**2**), $Cu(L^{I})_2$ (**3**), $Co(L^{II})_2$ (**4**), $Ni(L^{II})_2$ (**5**) and $Cu(L^{II})_2$ (**6**) complexes where $\mathbf{L^{I}}$ = 2-((E)-(5-(4-fluorophenyl)isoxazol-3-ylimino)methyl)-5-methoxyphenol and $\mathbf{L^{II}}$ = 2-((E)-(5-(4-fluorophenyl)isoxazol-3-ylimino)methyl)-4-bromophenol, were synthesized and characterized by FT–IR, UV–Vis, NMR, Mass, ESR, TGA, magnetic moment, SEM and powder XRD analyses. From the analytical results, all these metal(II) complexes are assigned to square planar geometry around the metal ions. The DNA binding and cleavage studies were evaluated for the synthesized compounds with CT–DNA and supercoiled pBR322 DNA respectively. All compounds have been monitored for their in the Vitro antimicrobial assay.

Keywords: Schiff base; Transition metal(II) complex; DNA interaction; Biological activity

1. Introduction

Nowadays, medicinal inorganic chemistry acquiring more importance as metal complexes offer possibilities for the design of anticancer agents due to interaction between transition metal complexes and DNA via non-covalent interactions such as electrostatic, groove and intercalative binding [1,2]. It is well known that the DNA is the important intracellular target for several drugs, which is evidenced by the interaction between the metal complexes and DNA leading to cell death by blocking the aggressive growth of cell division [3,4]. The existence of intercalative binding nature between metal complexes and DNA plays a key role in several clinical applications of the pharmaceutical field. Moreover, the presence of imine groups (−C=N) in Schiff bases and metal complexes are essential for the biological activities such as antimicrobial, antitumor and herbicidal properties, [5] and these compounds are interested in combined with bio-macromolecules due to the availability of aromatic nitrogen in its heterocyclic ring [6]. The compounds having planar ligands along with pi-delocalization systems have been reported as important DNA intercalators [7]. Most of the

transition metal complexes can induce the cleavage of DNA by oxidative and photolytic cleavage methods [8].

Cobalt is an essential constituent in coenzyme $B_{12,}$ and their complexes show significant biological properties viz., antimicrobial, antioxidant and antiviral [9]. Ni(II) complexes play a key role mainly in bioinorganic chemistry and some extent in redox enzyme systems. Palaniandavar et.al reported that the Cu(II) complexes are suitable replacements to cis-platin and act as anticancer agents [10,11]. Synthesis, spectral approach, antimicrobial activity, DNA binding and cleavage properties of metal complexes of various Schiff base ligands were reported from our laboratory [12-14]. In view of the above facts, in the present work, we have focused on the synthesis, structural characterization, antimicrobial activity, DNA binding and cleavage properties of M(II) complexes (**1-6**) from 3-amino-5-(4-fluoro phenyl) isoxazole Schiff base ligands.

2. Experimental

2.1. Materials and Instrumentation

$M(OAc)_2.xH_2O$ where (M= Co, Ni and Cu) other chemicals with analytical reagent grade purchased from Sigma–Aldrich Chemicals, Hi-Media Ltd., and Merck company. Solvents like acetone, methanol, chloroform, dichloromethane and pet ether were of analytical grade. These solvents were employed to purify by standard procedures before use. The Calf-thymus DNA (CT−DNA) and supercoiled pBR322 DNA was obtained from Genei, Bangalore, India and maintained at 4 ^{o}C temperature.

The NMR spectra of the Schiff bases were recorded on a Bruker 400 MHz NMR instrument, tetramethylsilane (TMS) was used as internal standard. Mass spectral data were analyzed by using a VG AUTOSPEC mass spectrometer at room temperature. Electronic absorption spectra in the range from 200 to 800 nm were recorded on Shimadzu UV–2600 spectrophotometer. Magnetic moment values of metal complexes were obtained by employing the Gouy balance model 7550. $Hg[Co(NCS)_4]$ was used as calibrant. Pascal constants are used for the diamagnetic corrections of the metal complexes. The polmon instrument, model No. MP–96 was employed to calculate the melting points of compounds. Infrared spectra of all these compounds were recorded on Perkin–Elmer Infrared model 337 in the range 4000–250 cm^{-1} with the help of KBr. The elemental analysis of the synthesized compounds were performed with Perkin-Elmer 240C (USA) elemental analyzer. The X-band ESR spectra of Cu(II) complexes were recorded in DMSO at 77 K (liq. Nitrogen temp.) on a

JES−FA200 ESR Spectrometer (JEOL–Japan). The thermal analyses (TGA) of complexes were determined in a dynamic nitrogen atmosphere with the help of Shimadzu TGA–50H instrument in the temperature range of 27–1000 ^{o}C. The heating rate is 10 ^{o}C min^{-1}. The surface morphology images of compounds were observed by using a JEOL, JSM–6360 LV scanning electron microscope, using a variable voltage between 15 and 20 kV at different magnifications. Powder XRD analysis of compounds was determined using Xpert Pro X–Ray Diffractometer. UV absorption studies and fluorescence quenching properties of synthesized complexes were investigated by Shimadzu UV–2600 spectrophotometer and spectrofluorometer model RF–5301PC (Shimadzu) respectively. Ostwald's viscometer (Vensil) was used to attain the viscosity measurements.

2.2. Synthesis of Schiff base ligands

The synthesis of $\mathbf{L^{I}}$ and $\mathbf{L^{II}}$ were shown in scheme I. The synthesis of Schiff bases carried out by slow addition of hot methanolic solution of 2-hydroxy-4-methoxybenzaldehyde / 2-hydroxy-5-bromobenzaldehyde (1.0 mmol) to hot methanolic solution of 3-amino-5-(4-fluorophenyl) isoxazole (1.0 mmol). The reaction mixture was refluxed for 2–3 hours at 60–70 ^{o}C, the mixture was allowed to cool for few hours. Under cool condition the coloured product was filtered and washed several times with cold methanol, pet ether and recrystallized. The purity of the Schiff bases was monitored using thin layer chromatography.

2.2.1. **Ligand $\mathbf{L^{I}}$:** Yield: 80%. M.P: 135-140 ^{o}C. M.Wt: 312. Analy. Calcd. ($C_{17}H_{13}FN_2O_2$): C, 65.38; H, 4.20; N, 8.97. Found: C, 65.12; H, 4.01; N, 8.68. FT−IR (KBr) (cm^{-1}): $\upsilon_{(OH)}$ 3441; $\upsilon_{(CH=N)}$ 1609; $\upsilon_{(C-O)}$ 1165. UV-Vis (DMSO) λ_{max}/nm (cm^{-1}): 261 (38314); 333 (30030). ^{1}H−NMR (400 MHz, $CDCl_3$): δ = 12.86 (s, 1 H), 8.84 (s, 1 H), 7.78-7.75 (m, 2 H), 7.30 (d, J = 8.28 Hz, 1 H), 7.18-7.14 (m, 2 H), 6.53-6.50 (m, 3 H), 3.84 (s, 3 H). ^{13}C−NMR (100 MHz, $CDCl_3$): δ = 170.1, 167.8, 166.6, 165.3, 164.2, 162.6, 134.7, 127.8, 127.7, 123.7, 116.3, 116.1, 112.4, 108.0, 101.0, 94.0, 55.5. Mass: *m/z* = 313 $[M+H]^{+}$.

2.2.2. **Ligand $\mathbf{L^{II}}$:** Yield: 78%. M.P: 175-180 ^{o}C. M.Wt: 360. Analy. Calcd. ($C_{16}H_{10}BrFN_2O_2$): C, 53.21; H, 2.79; N, 7.76. Found: C, 52.81; H, 2.52; N, 7.61. FT−IR (KBr) (cm^{-1}): $\upsilon_{(OH)}$ 3437; $\upsilon_{(CH=N)}$ 1617; $\upsilon_{(C-O)}$ 1175. UV-Vis (DMSO) λ_{max}/nm (cm^{-1}): 275 (36363); 349 (28653). ^{1}H−NMR (400 MHz, $CDCl_3$): δ = 12.40 (s, 1 H), 8.90 (s, 1 H), 7.81-7.78 (m, 2 H), 7.55-7.50 (m, 2 H), 7.22-7.17 (m, 2 H), 6.95 (d, J = 8.78 Hz, 1 H), 6.58 (s, 1 H). ^{13}C−NMR (100 MHz, $CDCl_3$): δ = 1170.6, 167.3, 166.6, 165.3, 162.8, 160.7, 137.4, 135.2, 127.9, 127.8, 123.5, 119.6, 116.5, 116.3, 110.9, 94.2. Mass: *m/z* = 359 $[M-H]^{+}$.

2.3. Synthesis of metal complexes [1–6]

Following procedure has been employed for the synthesis of metal complexes (M:L = 1:2 ratio). To the hot methanolic solution of Schiff bases ($\mathbf{L^{I}/L^{II}}$) (20 mM) added hot methanolic solution of appropriate metal acetates (M = Co, Ni & Cu) (10 mM) in a drop wise manner. After completion of addition, the reaction mixture refuted at 60–70 ^{o}C for 3–4 hours. The obtained solid coloured product was isolated, filters and washed with various solvents such as pet ether and cold methanol dried in vacuum desiccators over anhydrous $CaCl_2$. Scheme I represents the synthesis of Schiff base ligands and their metal complexes.

2.3.1. $[Co(L^{I})_2]$ (1): Yield: 76%. M.P: 250-256 ^{o}C. M.Wt: 682. Analy. Calcd: ($C_{34}H_{24}CoF_2N_4O_6$): C, 59.92; H, 3.55; N, 8.22. Found: C, 59.61; H, 3.31; N, 8.01. FT−IR (KBr) (cm^{-1}): $\upsilon_{(C=N)}$ 1590, $\upsilon_{(C-O)}$ 1159, $\upsilon_{(M-O)}$ 532, $\upsilon_{(M-N)}$ 402. UV-Vis (DMSO) λ_{max}/nm (cm^{-1}): 265 (37735), 295 (33898), 339 (29498), 395 (25316), 597 (16750). μ_{eff}(BM): 2.12. Mass (m/z): 721 $[M+K]^{+}$.

2.3.2. $[Ni(L^{I})_2]$ (2): Yield: 75%. M.P: 280-284 ^{o}C. M.Wt: 682. Analy. Calcd: ($C_{34}H_{24}NiF_2N_4O_6$): C, 59.94; H, 3.55; N, 8.22. Found: C, 59.62; H, 3.32; N, 8.03. FT−IR (KBr) (cm^{-1}): $\upsilon_{(C=N)}$ 1603, $\upsilon_{(C-O)}$ 1124, $\upsilon_{(M-O)}$ 531, $\upsilon_{(M-N)}$ 401. UV-Vis (DMSO) λ_{max}/nm (cm^{-1}): 266 (37593), 285 (35087), 337 (29673), 386 (25906), 610 (16393), 624 (16025). μ_{eff}(BM): Dia. Mass (m/z): 704 $[M+Na]^{+}$.

2.3.3.* $[Cu(L^{I})_2]$ *(3): Yield: 76%. M.P: 230-235 ^{o}C. M.Wt: 686. Analy. Calcd: ($C_{34}H_{24}CuF_2N_4O_6$): C, 59.52; H, 3.53; N, 8.17. Found: C, 59.23; H, 3.24; N, 8.02. FT−IR (KBr) (cm^{-1}): $\upsilon_{(C=N)}$ 1596, $\upsilon_{(C-O)}$ 1125, $\upsilon_{(M-O)}$ 538, $\upsilon_{(M-N)}$ 405. UV-Vis (DMSO) λ_{max}/nm (cm^{-1}): 268 (37313), 298 (33557), 324 (30864), 371 (26954), 588 (17006). μ_{eff}(BM):1.81. Mass (m/z): 686 $[M]^{+}$. ESR: $g_{\parallel}$=2.18, $g_{\perp}$=2.07, G=2.61.

2.3.4. $[Co(L^{II})_2]$ (4): Yield: 70%. M.P: 250-253 ^{o}C. M.Wt: 779. Analy. Calcd: ($C_{32}H_{18}Br_2CoF_2N_4O_4$): C, 49.32; H, 2.33; N, 7.19. Found: C, 48.95; H, 2.25; N, 7.01. FT−IR (KBr) (cm^{-1}): $\upsilon_{(C=N)}$ 1602, $\upsilon_{(C-O)}$ 1159, $\upsilon_{(M-O)}$ 520, $\upsilon_{(M-N)}$ 427. UV-Vis (DMSO) λ_{max}/nm (cm^{-1}): 262 (38167), 337 (29673), 411 (24330), 672 (14880). μ_{eff}(BM): 2.17. Mass (m/z): 780 $[M+H]^{+}$.

2.3.5. $[Ni(L^{II})_2]$ (5): Yield: 68%. M.P: 280-284 ^{o}C. M.Wt: 779. Anal. Calcd: ($C_{32}H_{18}Br_2NiF_2N_4O_4$): C, 49.34; H, 2.33; N, 7.19. Found: C, 49.05; H, 2.12; N, 7.00. FT−IR (KBr) (cm^{-1}): $\upsilon_{(C=N)}$ 1604, $\upsilon_{(C-O)}$ 1164, $\upsilon_{(M-O)}$ 516, $\upsilon_{(M-N)}$ 425. UV-Vis (DMSO) λ_{max}/nm

127 (cm^{-1}): 263 (38022), 337 (29673), 412 (24271), 660 (15151), 677 (14771). μ_{eff}(BM): Dia.
128 Mass (m/z): 779 $[M]^+$.

129 **2.3.6. $[Cu(L^{II})_2]$ (6):** Yield: 73%. M.P: 244-250 ^oC. M.Wt: 783. Anal. Calcd:
130 ($C_{32}H_{18}Br_2CuF_2N_4O_4$): C, 49.03; H, 2.31; N, 7.15. Found: C, 48.73; H, 2.10; N, 7.08. FT−IR
131 (KBr) (cm^{-1}): $\upsilon_{(C=N)}$ 1603, $\upsilon_{(C-O)}$ 1157, $\upsilon_{(M-O)}$ 518, $\upsilon_{(M-N)}$ 432. UV-Vis (DMSO) λ_{max}/nm
132 (cm^{-1}): 266 (37593), 346 (28901), 405 (24691), 671 (14903). μ_{eff}(BM):1.75. Mass (m/z): 784
133 $[M+H]^+$. ESR: $g_{\parallel}$=2.20, $g_{\perp}$=2.06, G=2.95.

134 ***3. Results and discussion***

135 Schiff base ligands and their metal complexes are coloured, stable at room temperature and
136 non-hygroscopic. The ligands are soluble in organic solvent like methanol, ethanol,
137 acetonitrile, chloroform, DMF and DMSO and their metal complexes are soluble in DMSO
138 and DMF only, whereas insoluble in alcohols and water. Analytical and spectral data is good
139 agreement with the formation of mononuclear Co(II), Ni(II) and Cu(II) complexes with 1:2
140 ratio (M:L).

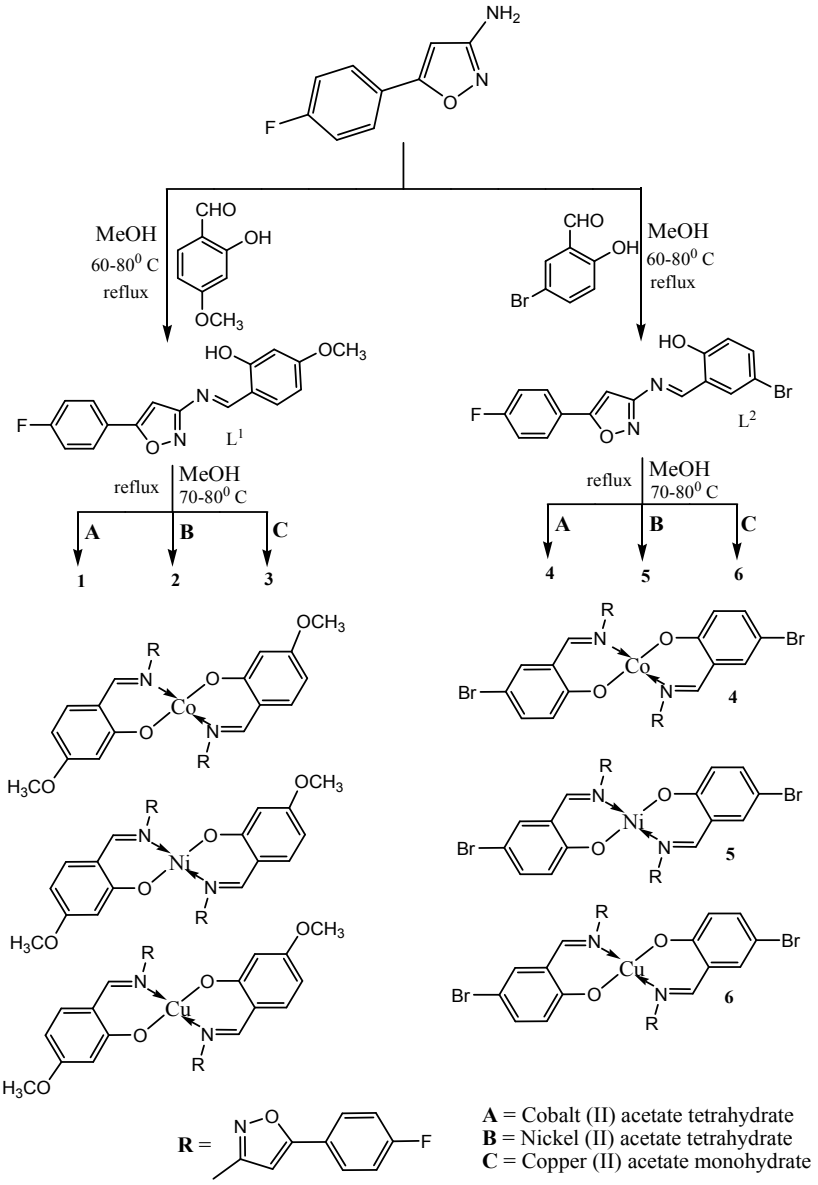

Scheme 1. Synthesis of Schiff bases and their metal(II) complexes.

3.1. FT–IR spectra

IR spectral analyses of metal complexes are correlated with the free Schiff base ligands to understand the coordination mode and binding sites upon complexation. Table 1 represents the characteristic IR data of synthesized complexes. The free ligands $\mathbf{L^I}$, $\mathbf{L^{II}}$ showed broad band at 3441, 3437 cm^{-1} respectively, due to phenolic –OH group [15,16], and these bands are disappeared in their metal complexes, represents the participation of phenolic oxygen in the formation of the metal complexes. Which is further confirmed by the shift in the $\nu_{(C-O)}$ bands at 1165, 1175 cm^{-1} of $\mathbf{L^I}$ and $\mathbf{L^{II}}$ ligands respectively, and these bands are decreases to lower

frequencies in their metal complexes [17]. The sharp absorption bands at 1609, 1617 cm^{-1} of the free ligands $\mathbf{L^I}$, $\mathbf{L^{II}}$ respectively, are assigned to the $\nu_{(C=N)}$. These bands are shifted to 13-19 cm^{-1} in their metal complexes [18], these is confirming the participation of nitrogen atom of azomethine group in coordination to the metal ion. The appearance of weak non-ligand bands in the metal complexes in the range 516−538 cm^{-1} and 401−432 cm^{-1} have been corresponding to $\nu_{(M-O)}$, $\nu_{(M-N)}$, respectively [19] (shown in Fig. 1).

Table 1. The FT–IR absorption frequencies (cm^{-1}) of the Schiff base ligands and their complexes

Compound	$\nu_{(OH)}$	$\nu_{(HC=N)}$	$\nu_{(C-O)}$	$\nu_{(M-O)}$	$\nu_{(M-N)}$
$\mathbf{L^I}$	3441	1609	1165	–	–
$Co(L^I)_2$ (**1**)	–	1590	1117	532	402
$Ni(L^I)_2$ (**2**)	–	1596	1124	531	401
$Cu(L^I)_2$(**3**)	–	1596	1125	538	405
$\mathbf{L^{II}}$	3437	1617	1175	–	–
$Co(L^{II})_2$(**4**)	–	1602	1159	520	427
$Ni(L^{II})_2$(**5**)	–	1604	1164	516	425
$Cu(L^{II})_2$ (**6**)	–	1603	1157	518	432

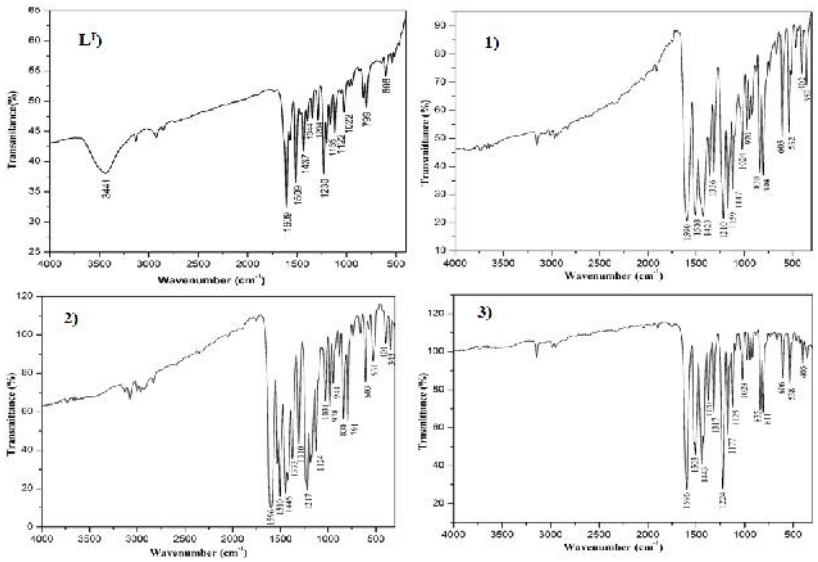

Fig.1. IR spectra of ligand L^I and its metal complexes.

3.2. Electronic spectra and magnetic susceptibility

Electronic absorption spectra of all compounds were investigated in DMSO solvent in the region 200–800 nm at room temperature. The absorption spectra of Schiff bases $\mathbf{L^I}$ and $\mathbf{L^{II}}$ exhibits two bands at 261–275 nm and 333–349 nm respectively. The absorption bands at

higher energies are presumably arising from π-π* transitions of aromatic benzene while the remaining lower energy bands are attributed to the n-π* transitions of the –C=N functional group. These transitions are shifted in metal complexes due to the coordination of the ligand with metal ion. The complexes also exhibited charge transfer bands in the range of 371-412 nm. The complexes **1** and **4** showed d–d bands at 597 nm and 672 nm respectively attributed to $^{1}A_{1g} \rightarrow {}^{1}B_{1g}$ transitions [20], and the magnetic moment values for the complex **1** & **4** found to be 2.12 BM and 2.17 BM respectively. Complexes **2** and **5** showed two d-d bands at 610 nm, 624 nm and at 660 nm, 677 nm, respectively, which were assigned to the spin allowed transitions $^{1}A_{1g} \rightarrow {}^{1}A_{2g}$, $^{1}A_{1g} \rightarrow {}^{1}B_{1g}$ for Ni(II) complexes [21]. These Ni(II) complexes show diamagnetic in nature. The complexes **3** and **6** displayed broad band at 588 nm and 671 nm respectively, attributable to $^{2}B_{1g} \rightarrow {}^{2}E_{g}$ for Cu(II) complexes [22,23]. The magnetic moment value of **3** is 1.81 BM and **6** is 1.75 BM, the absorption and magnetic susceptibility data concluded that the geometry around the metals is square-planar (shown in Fig.2).

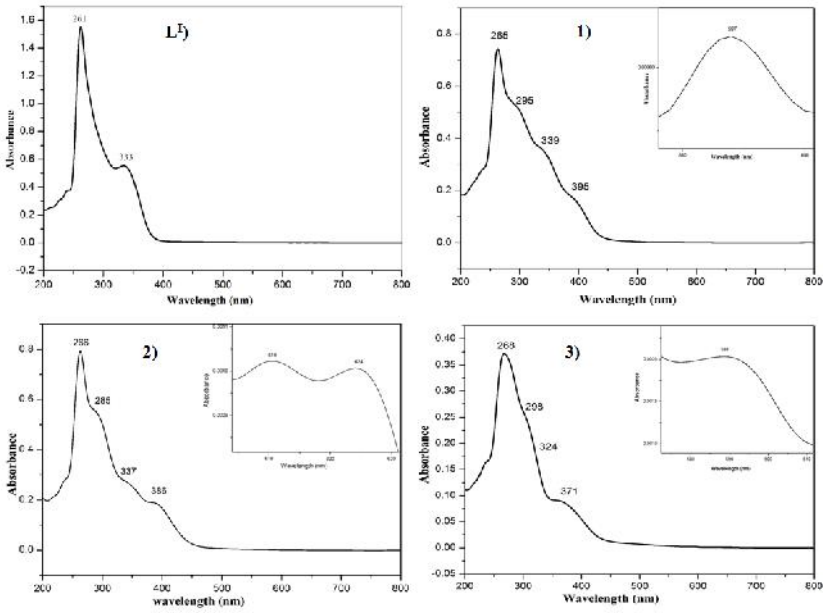

Fig.2. UV−Visible spectra of ligand L^{I} and its metal complexes

3.3. ESR spectra

The X-band Electron Spin Resonance (ESR) spectra of Cu(II) complexes were investigated in DMSO solvent at liquid nitrogen temperature (77K). The localization of unpaired electron in Cu(II) complexes (**3**, **6**) can be determined by electron spin resonance spectroscopy. Fig. 3 displayed the ESR spectrum of complex **3**. The values of ESR parameters $g_{\parallel}$, $g_{\perp}$ and G for

complex **3** are found to be 2.18, 2.07 and 2.61 respectively, for complex **6** are 2.20, 2.06 and 2.95. The "*g*" tensor values of the **3**, **6** complexes are found to be $g_{\parallel} > g_{\perp} > g_e$ (2.0023). This order suggests that the single/unpaired electron is localized in the $d_{x^2-y^2}$ orbital of Cu(II) complex having square planar geometry [24]. The $g_{\parallel}$ values of Cu(II) complexes (**3** and **6)** are found to be 2.18 and 2.20 respectively suggesting the complexes are covalent in nature [25]. The G values of complex **3** (2.61) and complex **6** (2.95) suggesting the Cu−Cu ion exchange interactions are considerable.

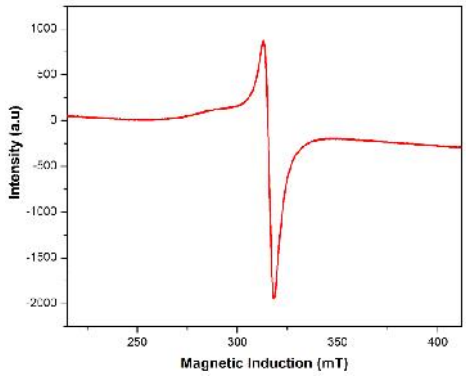

Fig.3. ESR spectrum of complex 3.

3.4. Mass spectral studies

The mass spectral analysis of Schiff base ligands and their respective metal complexes (**1**–**6**) were recorded at room temperature. The proposed formulae for the Schiff base ligands and their respective complexes were confirmed by molecular ion peaks obtained. The mass spectra of Schiff base ligands $\mathbf{L^I}$, $\mathbf{L^{II}}$ and complexes **1**−**6** show the molecular ion peaks at m/z = 313 $[M+H]^+$, 359 $[M+H]^+$, 721 $[M+K]^+$, 704 $[M+Na]^+$, 686 $[M]^+$, 780 $[M+H]^+$, 779 $[M]^+$, 784 $[M+H]^+$ respectively. The molecular ions of metal complexes are in good agreement with 1:2 (metal: ligand) stoichiometric ratio.

3.5. Thermal analysis

The thermal stability of metal complexes (**1**–**6**) was analyzed by thermogravimetric analysis (TGA). The thermal analysis of the sample was determined in a platinum pan under N_2 atmosphere. The heating rate was linearly increased at 10 $^oC\ min^{-1}$ over a temperature range 27–1000 °C. The two step pyrolysis was observed in thermograms of metal complexes (**1**–**6**). The decomposition of these metal complexes begins from 250-260 ^oC which confirms that these metal complexes are free from coordinated water molecules. The initial step decomposition may be due to the partial loss of ligand around 250–310 ^oC and the second phase decomposition is attributed to the loss of total organic portion at 260–600 ^oC

212 temperature range and above 600 ^{o}C complete decomposition of complexes occurred,
213 resulting in metal oxide (MO) as final residue. The thermograms of complexes **1**, **2** and **3**
214 were presented in Fig.4.

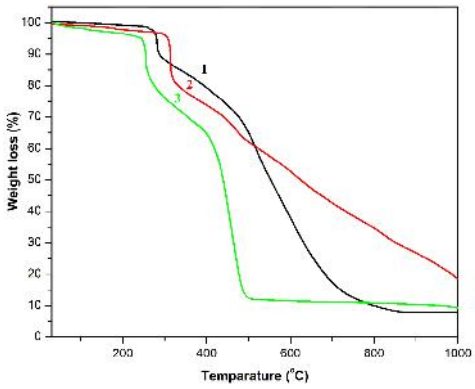

215

216 **Fig.4.** Thermal analysis curves of complexes 1, 2 and 3.

217 **3.6. XRD**

218 The nature of synthesized compounds was determined by powder XRD analysis as it was
219 difficult to segregate the suitable single crystals for X–ray crystallographic studies. The
220 powder XRD patterns of Schiff base ($\mathbf{L^{I}}$) and their complexes (**1**, **2** and **3**) are shown in Fig. 5
221 and exhibit sharp peaks, represent their crystalline nature. The grain sizes of all synthesized
222 compounds were calculated by applying the Debye-Scherrer's equation

223 $$D = 0.9\,\lambda / \beta \cos\theta \qquad \text{----------} \qquad (1)$$

224 Where D = particle size, 0.9 is the shape factor constant, λ = wavelength of X–ray radiation,
225 β = full width at the half-maximum (FWHM) and θ = diffraction angle for hkl plane. Finally,
226 the grain sizes of all compounds were found as 30.8 nm ($\mathbf{L^{I}}$), 46.4 nm ($\mathbf{L^{II}}$), 38.2 nm (**1**), 25.2
227 nm (**2**), 22.4 nm (**3**), 22.1 nm (**4**), 34.9 nm (**5**) and 20.1 nm (**6**).

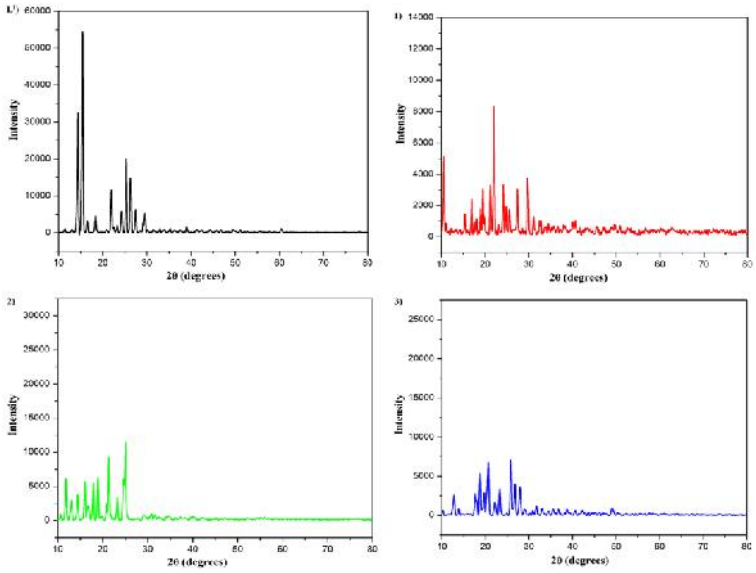

Fig.5. Powder XRD patterns of L^I and its complexes 1, 2 and 3.

3.7. SEM

The surface morphological difference between Schiff base ligands and their respective complexes were evaluated by scanning electron microscope analysis (SEM). SEM analysis showed a significant morphological difference between ligands and their metal complexes due to the coordination of donor sites of the Schiff base ligands to the metal ions [26], and the surface morphology of metal complexes changed by changing the metal ions. The SEM photographs of compounds shown in Fig.6. The micrographs of ligands (**L^I, L^{II}**) depict irregular small broken pieces of wood like structures and a vertically cut layer of rock like structure respectively. These facts revealed the amorphous nature of the ligands with unclear appearance. The SEM micrographs of metal complexes (**1**–**6**) explained as follows, the micrograph of complex **1** indicates the non-uniform crystal like structures of variable lateral dimensions along with some scattered rods. Complex **2** indicates the unclear appearance of platelet-like structures and the complex **3** indicates presence of nanoneedles and rods with the gorgeous surface. Here, in these three metal complexes, it is found to be surface morphology is different, due to the presence of various metal ions. However, the complex **4** shows smooth surfaced nanorod-like structures. Well defined smaller and larger rod-like particles of different size were observed in complex **5,** and the complex **6** has a twisted fiber and grass like morphology.

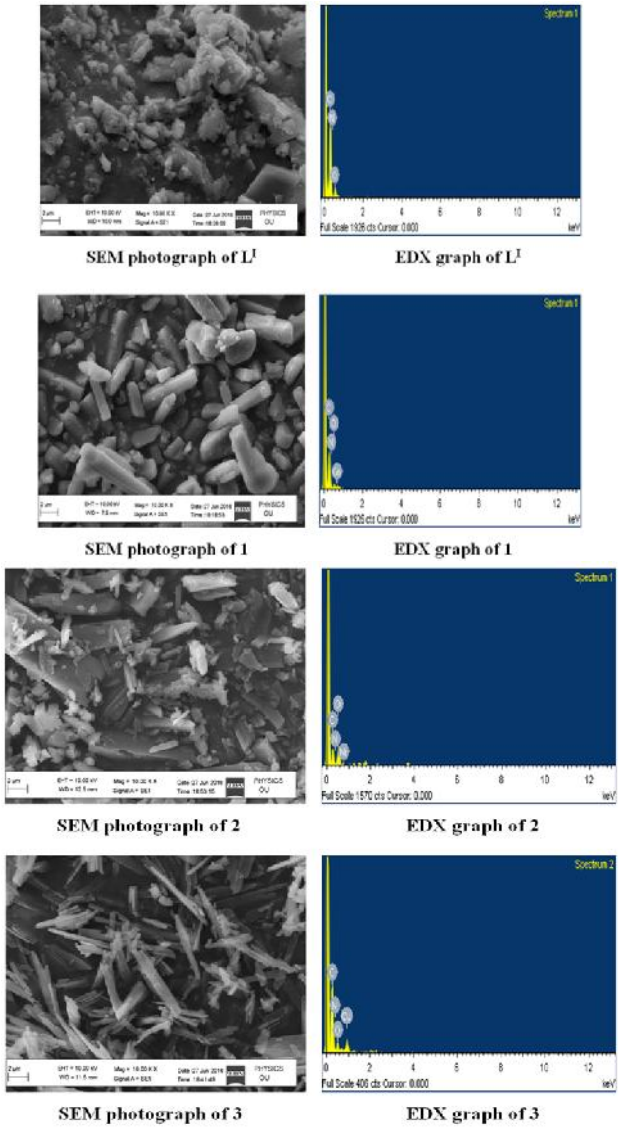

Fig.6. SEM and EDX graphs of L^I and its complexes1, 2 and 3.

3.8. DNA binding and cleavage experiments

3.8.1. UV–Vis absorption study

DNA is known to an important pharmacological target for various chemotherapeutic drugs, so, the interaction between metal complexes and CT–DNA is of vital in understanding the binding mechanism [27]. Binding nature of the metal complexes and CT–DNA was determined by electronic absorption spectroscopy technique [28]. Stepwise increment of CT–DNA to analyzed metal complex may produce the change in the UV absorption of metal complexes which serves as a substantial proof of the existence of an interaction between DNA base pairs and aromatic chromophore of analyzed compounds. In the present

investigation, hypochromism is observed in the absorption spectral curves with a red-shift (bathochromism), leads to stabilization of DNA–metal complex adduct. The stacking interactions between the DNA base pairs and an aromatic chromophore are responsible for the hypochromism and bathochromic shift [29]. Metallo–intercalators are metal complexes possessing ligands containing aromatic planar groups and these ligands are oriented in such a way that protruding away from the central metal ion and situated in a parallel manner to the DNA base pairs, can readily π-stack in DNA double helix. Generally, in such metal complexes, the core metal ion also comes under planar portion [30]. The compounds are bind to DNA base pairs, and this interaction occurred between the π* orbital of the metal complexes and π orbital of the DNA base pairs, and the transition energies of π-π* orbital decreased. The transition probabilities are decreased due to the coupled π* orbitals were partially filled with electrons [31]. The hypochromism property in the absorption spectra depends on intercalative binding strength. In the present study, the spectra of metal complexes (**1**–**6**) show absorption bands in the range 263–270 nm attributed to π-π* transition bands. On gradual increments of CT–DNA, the π-π* transition band intensity reduces by 13–28% (hypochromism) in association with a bathochromic shift of 2–3 nm, shown in Fig. 7. The following equation was used for the determination of 'K_b' values of DNA complex adduct.

$$[DNA]/(\varepsilon_a-\varepsilon_f) = [DNA]/(\varepsilon_b-\varepsilon_f) + 1/K_b(\varepsilon_b-\varepsilon_f) \quad \text{----------} \quad (2)$$

Where [DNA] = concentration of DNA in the base pairs, K_b = intrinsic binding constant, ε_a is the apparent coefficient of A_{obsd}/[complex], ε_f and ε_b are the extinction coefficients of the free and fully bound forms of the complex, respectively. The intrinsic binding constant (K_b) values are found to be $4.38\pm0.02\times10^4$ M^{-1} (**1**), $7.83\pm0.01\times10^4$ M^{-1} (**2**), $2.17\pm0.01\times10^5$ M^{-1} (**3**), $2.85\pm0.02\times10^4$ M^{-1} (**4**), $8.91\pm0.01\times10^4$ M^{-1} (**5**) and $1.55\pm0.02\times10^5$ M^{-1} (**6**). The above K_b values conclude that the Cu(II) complexes are strongly interacting with CT−DNA than the Co(II) and Ni(II) complexes.

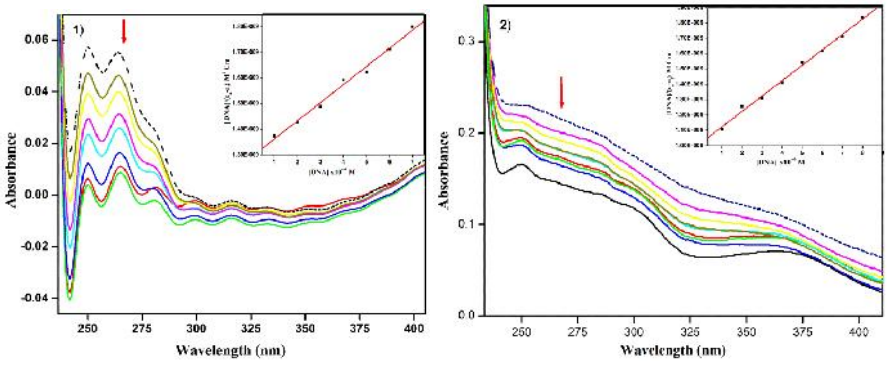

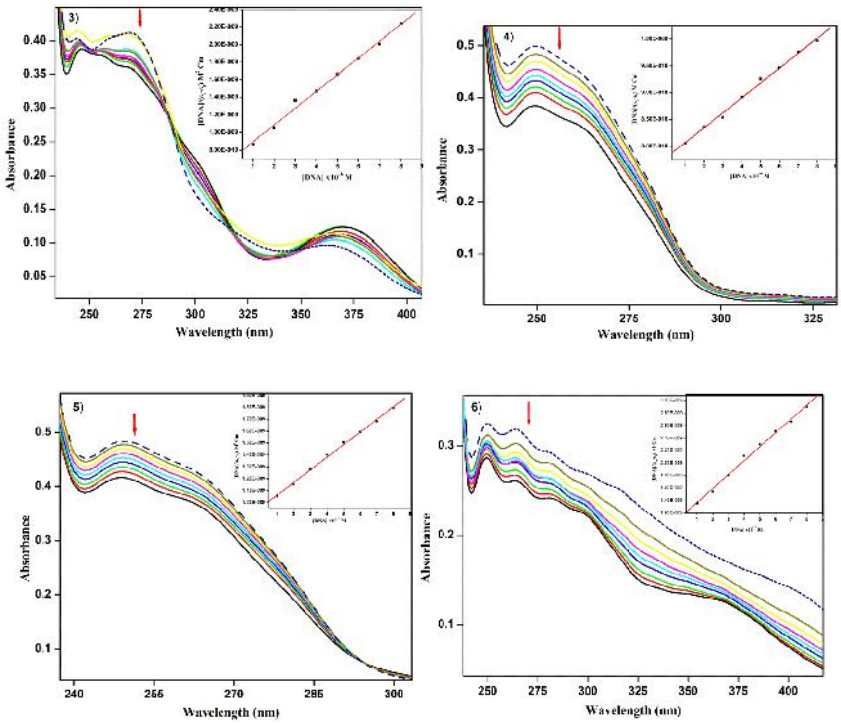

Fig.7. UV-Vis absorption spectra of complexes in the absence (dashed line) and presence (solid lines) of increasing concentrations of CT–DNA in Tris–HCl/NaCl buffer (pH 7.2). Arrow (↓) shows the hypochromic and bathochromic shift upon increase of the CT–DNA concentration. Inset: linear plot, [DNA]/ (ε_a–ε_f) Vs [DNA] give the intrinsic binding constant, K_b.

3.8.2. Fluorescence quenching study

The intercalative binding mode between metal complexes and CT–DNA was further evidenced by fluorescence quenching studies. In Tris–HCl/NaCl buffer (pH 7.2) EB is non-emissive due to the solvent molecules can quench the fluorescence nature of free EB. It is well known that in association with CT–DNA, EB can show enlarged emission intensity, this is because of strong intercalative binding nature between EB and adjacent DNA base pairs [32]. The enhanced emission intensity can be quenched by the successive addition of metal complexes, which can bind with CT–DNA through intercalative binding mode by displacing EB. The decrease in fluorescence intensity of EB was observed with raising in metal complexes concentration, which suggests the competitive binding between title compounds and EB to bind with DNA, with this the extent of emission quenching was observed, and it provides a clue to investigate the extent of binding of metal complexes with DNA. The EB, CT–DNA system shows, the fluorescence intensities at 590 nm reduced with the gradual

increment of metal complex concentration, which indicates that the metal complexes could bind the CT–DNA at the intercalation sites by displacing the EB. Classical Stern–Volmer equation [33,34], was employed to calculate the binding interactions of metal complexes **(1−6)** with CT–DNA.

$$I_0/I = 1 + K_{sv}[Q] \qquad \text{----------} \qquad (3)$$

Where I_0 = fluorescence intensity in the absence of complex and I = fluorescence intensity in the presence of complex, K_{sv} is a Stern–Volmer constant which is a measure of the efficiency of quenching and [Q] = [metal complex] (concentration of quencher). Apparent binding constant (K_{sv}) values are evaluated from the slope of I_0/I Vs [Q] and found to be $5.58\pm0.02\times10^3$ M^{-1} (**1**), $1.38\pm0.02\times10^4$ M^{-1} (**2**) $1.48\pm0.02\times10^4$ M^{-1} (**3**), $2.89\pm0.02\times10^3$ M^{-1} (**4**), $3.09\pm0.01\times10^3$ M^{-1} (**5**) and $1.42\pm0.01\times10^4$ M^{-1} (**6**) suggesting the stronger affinity of these metal complexes to CT–DNA shown in fig.8. The above K_{sv} values confirmed that the Cu(II) complexes are having more fluorescence quenching ability than the Co(II) and Ni(II) complexes. These results are well consistent with the UV–Vis absorption results.

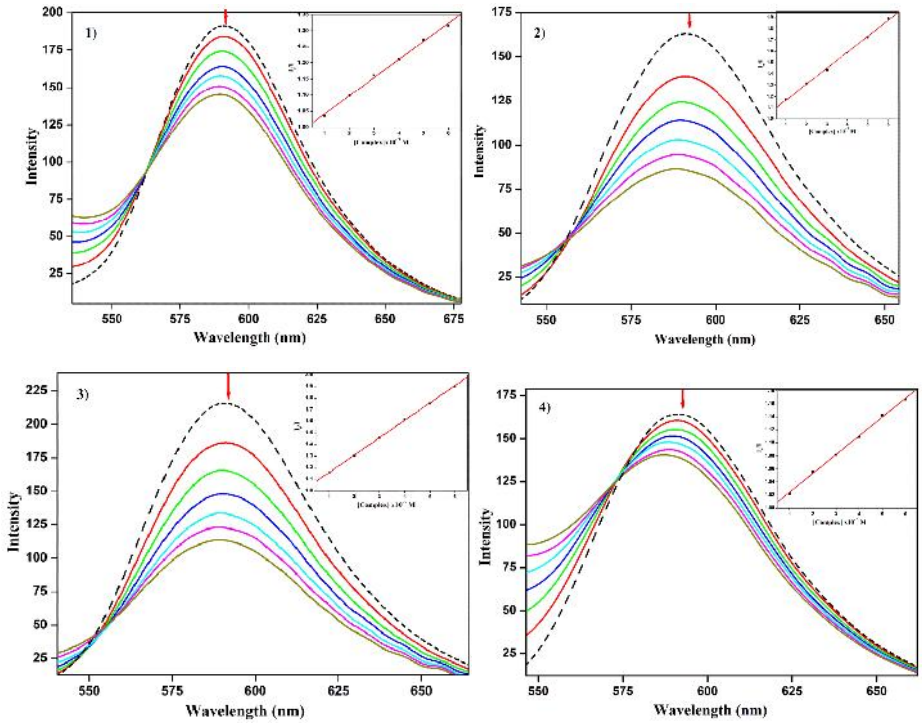

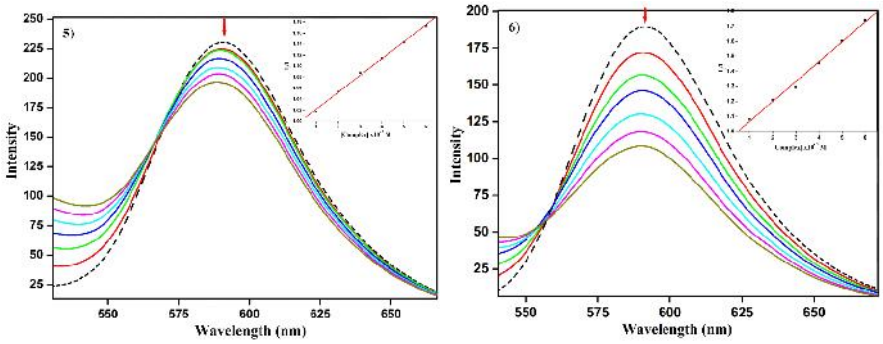

Fig.8.Changes in the fluorescence emission spectra of CT–DNA and EB bound complex in Tris–HCl/NaCl buffer (pH = 7.2) at 27 ^{o}C, in the absence (dashed line) and presence (solid lines) of increasing concentrations of the complexes (**1**–**6**). Inset: the plot of emission intensity I_0/I Vs [complex].

3.8.3. Viscosity measurements

To observe the binding mode and binding intensity of all synthesized complexes with DNA, the viscosity measurement technique was also employed. Hydrodynamic measurements (i.e., viscosity and sedimentation) are sensitive to DNA length. Intercalators (e.g., EB) are expected to lengthen the DNA helix. This lengthening is due to insertion of compounds in between the gaps of DNA–base pairs with this reason the viscosity of DNA was increased [35]. Fig. 9 shows the change in viscosity changes of CT−DNA by metal complexes (**1**–**6**) in combination with the change from classical intercalator, Ethidium bromide. The metal complexes intercalate between the DNA base pairs and increase the distance between the DNA base pairs where the compound was attached (intercalation site), leads to raising in DNA viscosity. The viscosity of CT–DNA, and the binding style between the CT–DNA and added metal complex was determined in the presence of variable quantities of metal complexes. The experimental results showed the increase relative viscosity of CT–DNA with the successive addition of complexes. Moreover, the increased viscosity of DNA clearly suggests that the metal complexes bind to DNA via an intercalation mode [36]. The viscosity measurements disclose that the increase is more in the case of Cu(II) complexes (**3**, **6**) suggesting Cu(II) complexes are more effective intercalate with CT–DNA than Co(II) and Ni(II) complexes, these results are consistent with previously obtained UV–Vis absorption and fluorescence results.

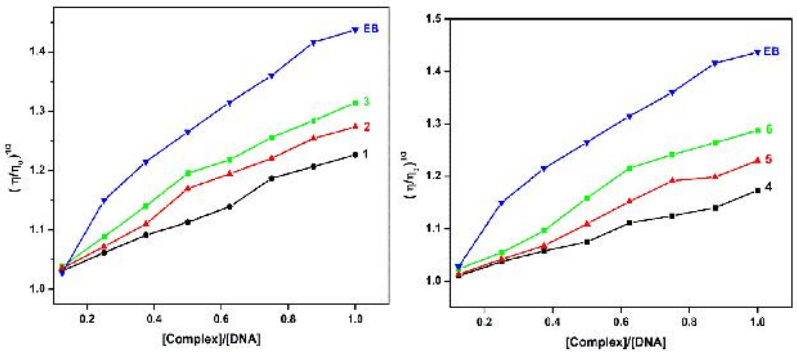

Fig.9. Viscosity measurements of the EB and complexes **1**–**6**.

3.8.4. DNA cleavage experiments

It is necessary to study the cleavage activity for the development of novel artificial nucleases and to understand the cleavage mechanism of nuclease to DNA. The chemical–DNA nuclease capacity is controlled by conversion of pBR322 DNA (supercoiled) into nicked circular and linear forms of DNA. In gel electrophoresis of pBR322 DNA, it is found that the fastest movement is noticed for supercoiled form DNA (Form I), the slowest moment is observed for the nicked form (Form II) due to cleavage of one strand. A linear form (Form III) is generated by cleavage of both strands of DNA, it is migrated between the Form I and Form II [37].

In the present study, other than Schiff bases, all the synthesized metal complexes showed better DNA cleavage property in combination with H_2O_2 and UV light. Fig. 10 shows the cleavage property of $\mathbf{L^I}$ ligand and its metal complexes (**1**, **2** & **3**) against pBR322 DNA in the presence of H_2O_2 and UV light. In oxidative cleavage, no apparent cleavage is found in lane 1(control) and lane 2 (DNA+ H_2O_2). The ligand alone is also inactive in cleaving the DNA under similar reaction conditions which are shown in lane 3 ($\mathbf{L^I}$), and the lane 4 (**1**) effectively cleaved the supercoiled DNA into Form II & III, the lane 5 (**2**) and lane 6 (**3**) are cleaved the supercoiled DNA into Form II. The mechanism of oxidative cleavage with metal complexes is shown in Scheme II. In Photolytic cleavage, the DNA cleavage property is not observed in lane 1 (control) and lane 2 ($\mathbf{L^I}$) but lane 3 (**1**) cleaved the DNA into form II and the lane 4 (**2**), lane 5 (**3**) cleaved the DNA into Form II & III. The effective cleavage capacity is observed in an oxidative method in comparison with the photolytic method. The gel electrophoresis results revealed that the complexes **1**, **2**, **3** show efficient cleavage ability than the **4**, **5**, **6** (Fig. 11) complexes.

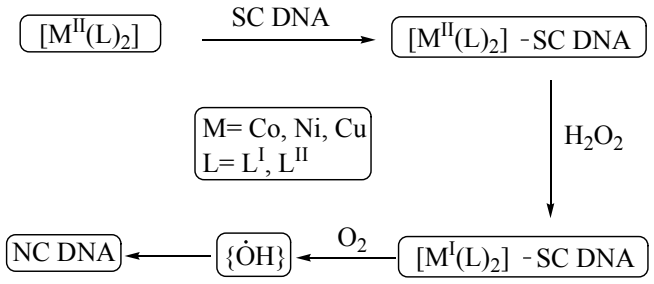

Scheme 2. An oxidative cleavage of DNA by Co(II), Ni(II) and Cu(II) complexes (1–6) in association with H_2O_2 as possible mechanism

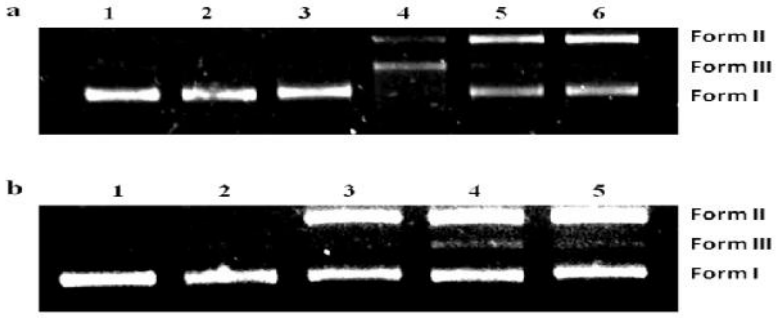

Fig.10. (a) Oxidative cleavage of supercoiled pBR322 DNA (0.2 μg, 33.3 μM) at 37 °C in 5mM TrisHCl/5 Mm NaCl buffer by the metal complexes. Lane 1, DNA control; Lane 2, DNA +H_2O_2 (1mM); Lane 3, DNA + H_2O_2 (1mM) + L^I (20 μM); Lane 4, DNA + H_2O_2 (1mM) + 1 (20 μM); Lane 5, DNA + H_2O_2 (1mM) + 2 (20 μM); Lane 6, DNA + H_2O_2 (1mM) + 3 (20 μM). **(b)** Photolytic cleavage of supercoiled pBR322 DNA (0.2 μg, 33.3 μM) at 37 °C in 5mM TrisHCl/5 mMNaCl buffer by the complexes. UV irradiation of wavelength is 365 nm. Lane 1, DNA control; Lane 2 DNA + L^I (20 μM); Lane 3, DNA + 1 (20 μM); Lane 4, DNA + 2 (20 μM); Lane 5, DNA + 3 (20 μM).

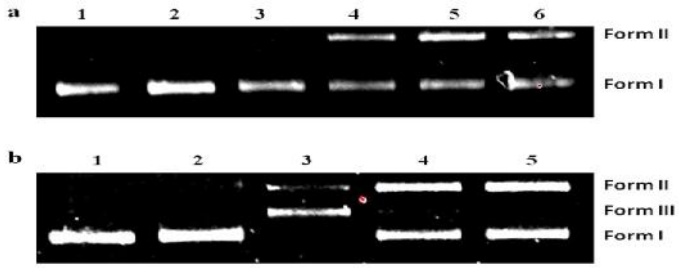

Fig.11. (a) Oxidative cleavage of supercoiled pBR322 DNA (0.2 μg, 33.3 μM) at 37 °C in 5mM TrisHCl/5 mM NaCl buffer by the metal complexes. Lane 1, DNA control; Lane 2, DNA +H_2O_2 (1mM); Lane 3, DNA + H_2O_2 (1mM) + L^{II} (20 μM); Lane 4, DNA + H_2O_2

(1mM) + 4 (20 μM); Lane 5, DNA + H_2O_2 (1mM) + 5 (20 μM); Lane 6, DNA + H_2O_2 (1mM) + 6 (20 μM). **(b)** Photoactivated cleavage of supercoiled pBR322 DNA (0.2 μg, 33.3 μM) at 37 °C in 5mM TrisHCl/5 mMNaCl buffer by the complexes UV irradiation of wavelength 365 nm. Lane 1, DNA control; Lane 2 DNA + L^{II} (20 μM); Lane 3, DNA + 4 (20 μM); Lane 4, DNA + 5 (20 μM); Lane 5, DNA + 6 (20 μM).

3.9. Antimicrobial activity

In vitro, biological screening activities of Schiff base ligands and their complexes were investigated against bacterial and fungal strains. After incubation of bacterial (24 h) and fungal (72 h) cultures at 30 ^{o}C, the inhibition zone values (in mm) are calculated, and the data is given in Table 2. The antibacterial and antifungal results of Schiff base ligands (**L^{I}**, **L^{II}**) and their metal complexes (**1**–**6**) represented the metal complexes showed more antimicrobial activity than free ligands. The graphs (Fig. 12) show a zone of inhibition area of antibacterial and antifungal activity of all compounds. The enhancement of antimicrobial activity is due to –C=N group and chelation effect with a metal ion in complexes [38]. This enhanced antimicrobial activity nature of metal complexes was demonstrated by Overtone [39] and chelation theory by Tweedy [40]. Overtone explained by cell permeability, according to this concept the cell is surrounded by lipid membrane which allows only lipid soluble compounds to pass through it, thereby controlling the microbial activity which causes the cell death. Moreover, the metal ion loses its polarity transferring of its positive charge to the donor groups [41]. This procedure enhances the lipophilic character of the metal ion. This lipophilic character increases its permeable capacity and penetrates more potently into the microorganism via lipid membrane, and thus they have killed aggressively [42].

Table 2. Antimicrobial activity result of Schiff bases and their metal complexes at 1mg/mL concentration

Compound	**Bacteria (mm)**				**Fungi (mm)**	
	Gram-positive bacteria		**Gram-negative bacteria**		***S. rolfsii***	***M. phaseolina***
	B. amyloliquefaciens	***S. aureus***	***E. coli***	***P. aeruginosa***		
L^{I}	9	10	7	9	10	8
$Co(L^{I})_2$ (**1**)	15	16	13	15	16	15
$Ni(L^{I})_2$ (**2**)	19	20	18	21	20	18
$Cu(L^{I})_2$(**3**)	24	23	25	22	24	23
L^{II}	10	9	8	10	7	9
$Co(L^{II})_2$(**4**)	12	14	12	13	14	12

$Ni(L^{II})_2$(**5**)	17	18	16	17	18	16
$Cu(L^{II})_2$(**6**)	22	21	22	20	21	21
Streptomycin	31	31	30	33	–	–
Mancozeb	–	–	–	–	30	31

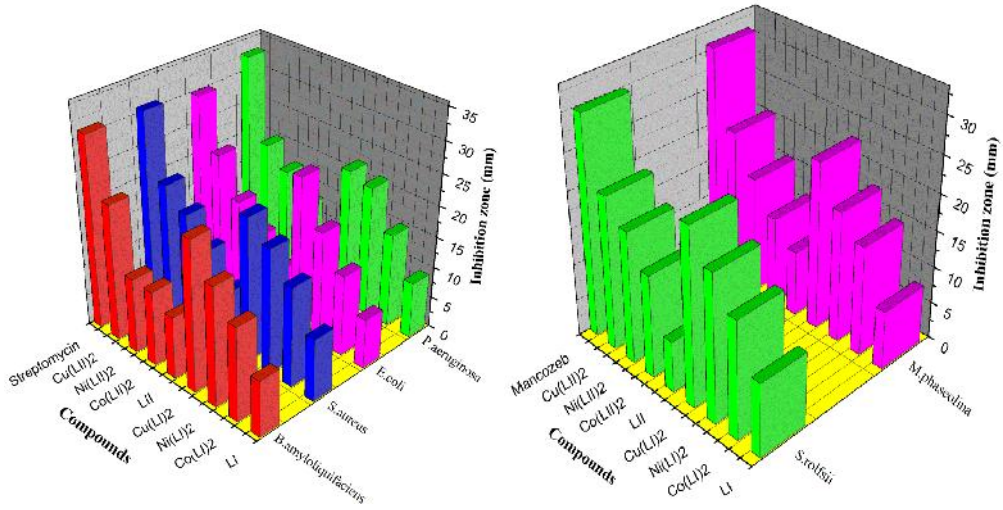

418

419 **Fig.12.** Zone of inhibition (in mm) of ligands and their complexes (1−6) tested against
420 bacterial and fungal strains.

421 **4. Conclusion**

422 Aiming towards the development of new metal-based drugs, a series of biologically
423 important metal complexes have been synthesized using $\mathbf{L^I}$, $\mathbf{L^{II}}$ Schiff base ligands. The
424 ligands and their complexes $Co(L^I)_2$ (**1**), $Ni(L^I)_2$ (**2**), $Cu(L^I)_2$ (**3**), $Co(L^{II})_2$ (**4**), $Ni(L^{II})_2$ (**5**) and
425 $Cu(L^{II})_2$ (**6**) have been analysed with various spectroscopic methods. According to analytical
426 data, a square planar geometry is attributed to these metal complexes. Powder XRD analysis
427 calculated grain sizes of all compounds and the surface morphologies of all compounds were
428 evaluated by Scanning electron microscope analysis. The SEM analysis showed a significant
429 morphological difference between ligands and their metal complexes. The interactions
430 between the metal complexes and CT−DNA have been determined by absorption,
431 fluorescence quenching studies, and viscosity measurements. From these results, it is
432 observed that the nature of binding is found to be an intercalative mode. The DNA cleavage
433 properties were examined against pBR322 DNA by using these metal complexes in
434 combination with H_2O_2 as well as UV light, and the results showed that the metal complexes
435 effectively cleaved than the free Schiff base ligands. The antimicrobial activity of ligands and
436 their metal complexes was carried out against bacterial & fungal strains, it is observed that all

437 the metal complexes showed good antimicrobial activity compared to free Schiff base
438 ligands.
439
440 **References**

441 1. Hambley TW, Developing new metal-based therapeutics: challenges and
442 opportunities, *Dalton Trans.* 2007;21**:** 4929.
443 2. Raman N, Joseph J, Velan A S K, Pothiraj C, Antifungal Activities of Biorelevant
444 Complexes of Copper(II) with Biosensitive Macrocyclic Ligands, *Mycobiology,*
445 2006;34:*214.*
446 3. Metcalfe C, Thomas J A, Kinetically inert transition metal complexes that reversibly
447 bind to DNA, *Chem. Soc. Rev.* 2006;32: 215.
448 4. Rad F V, Housaindokht M R, Jalal R, Hosseini H E, Doghaei A V, Goghari S S,
449 Spectroscopic and Molecular Modeling Based Approaches to Study on the Binding
450 Behavior of DNA with a Copper (II) Complex, *J. Fluoresc.* 2014;24: 1225.
451 5. Antony R, Manickam S T D, Saravanan K, Karuppasamy K, Balakumar S Synthesis,
452 spectroscopic and catalytic studies of Cu(II), Co(II) and Ni(II)complexes immobilized
453 on Schiff base modified chitosan *J. Mol. Struct.* 2013;1050:53.
454 6. Wang L H, Gou S H, Chen Y J, Liu Y, Potential new antitumor agents from an
455 innovative combination of camphorato, a ramification of traditional Chinese
456 medicine, with a platinum moiety, *Bioorg. Med. Chem. Lett.* 2005;15:3417.
457 7. Daravath S, Kumar M P, Rambabu A, Vamsikrishna N, Ganji N, Shivaraj, The
458 preparation and characterisation of cyclam/anthraquinone macrocycle/intercalator
459 complexes and their interactions with DNA, *J. Mol. Struc.* 2017;1144:147.
460 8. Burrows C J, Muller J G, Oxidative Nucleobase Modifications Leading to Strand
461 Scission Scission. *Chem. Rev.* 1998;98:1109.
462 9. Bottcher A, Takeuchi T, Hardcastle K I, Meade T J, GrayH B, Spectroscopy and
463 Electrochemistry of Cobalt(III) Schiff Base Complexes, *Inorg. Chem.* 1997;36:2498.
464 10. Shafaatian B, Soleymanpour A, Oskouei N K, Notash B, Rezvani S A, Synthesis,
465 crystal structure, fluorescence and electrochemical studies of a new tridentate Schiff
466 base ligand and its nickel(II) and palladium(II) complexes, *Spectro chimica. Acta A.*
467 2014;128:363.
468 11. Ramakrishnan S, Shakthipriya D, Suresh E, Periasamy V S, Akbarsha M A,
469 Palaniandavar M, Ternary Dinuclear Copper(II) Complexes of a Hydroxybenzamide

Ligand with Diimine Coligands: the 5,6-dmp Ligand Enhances DNA Binding and Cleavage and Induces Apoptosis, *Inorg. Chem.* 2011;50:6458.

12. Kumar M P, Vamsikrishna N, Ramesh G, Subhashini N J P, Nanubolu J B, Shivaraj Cu(II) complexes with 4-amino-3,5-dimethyl isoxazole and substituted aromatic aldehyde Schiff bases: Synthesis, crystal structure, antimicrobial activity, DNA binding and cleavage studies, *J. Coord. Chem.* 2017;70:1368.
13. Vamsikrishna N, Kumar M P, Tejaswi S, Rambabu A, Shivaraj, DNA Binding, Cleavage and Antibacterial Activity of Mononuclear Cu(II), Ni(II) and Co(II) Complexes Derived from Novel Benzothiazole Schiff Bases. *J. Fluoresc.* 2016;26:1317.
14. Tejaswi S, Kumar M P, Rambabu A, Vamsikrishna N, Shivaraj, Synthesis, Structural, DNA Binding and Cleavage Studies of Cu(II) Complexes Containing Benzothiazole Cored Schiff Bases, *J. Fluoresc.* 2016;26:2151.
15. Marmur J, A procedure for the isolation of deoxyribonucleic acid from Microorganisms *J. Mol. Biol.* 1961;3:208.
16. Nakamoto fifth ed., Infrared and Raman Spectra of Inorganic and Coordination Compounds, Wiley-Interscience, New York. 1997.
17. Saydam S, Yilmaz E, Synthesis, characterization and thermal behavior of 4-chloromethyl-2-(2-hydroxybenzilidenehydrazino) thiazole and its complexes with Cr(III), Co(II), Ni(II) and Cu(II), Spectrochimica. Acta 2006;63:506.
18. Ray A, Rosair G M, Kadam R, Mitra S, Three new mono–di–trinuclear cobalt complexes of selectively and non-selectively condensed Schiff bases with N2O and N2O2 donor sets: Syntheses, structural variations, EPR and DNA binding studies, *Polyhedron,* 2009;28:796.
19. Ayman A, Abdel A, Microwave-Assisted Synthesis of Mn(II), Co(II), Ni(II), Cu(II), and Zn(II) Complexes of Tridentate Schiff Base N-(2-hydroxyphenyl) 2-hydroxy-5-bromobenzaldimine: Characterization, DNA Interaction, Antioxidant, and In Vitro Antimicrobial Studies, *Synth. React. Inorg. Met-Org. Nano Met. Chem.* 2014;44:1137.
20. Garg B S, Sharma R K, Kundra E, Copper(II), nickel(II), cobalt(II) and zinc(II) complexes of 2-[2-(6-methylbenzothiazolyl)azo]-5 dimethylaminobenzoic acid: synthesis, spectral, thermal and molecular modelling studies, *Transition Met. Chem.* 2005;30:552.

21. Cotton F A, Wilkinson G, Murillo C A, Bachmann M, Advanced Inorganic Chemistry, sixth ed., Wiley., New York. 2003.
22. Kathiresan S, Anand T, Mugesh S, Annaraj J, Synthesis, spectral characterization and DNA bindings of tridentate N2O donor Schiff base metal(II) complexes *J. Photochem. Photobiol. B* 2015;148:290.
23. Bahaffi S O, Aziz A A A, El-Naggar M M, Synthesis, spectral characterization, DNA binding ability and antibacterial screening of copper(II) complexes of symmetrical NOON tetradentate Schiff bases bearing different bridges, *J. Mol. Str.* 2012;1020:188.
24. Hathaway B J, Tomlinson A A G, Copper(II) ammonia complexes, *Coord. Chem. Rev.* 1970; 5 1.
25. Patel R N, Singh N, Shukla K K, Chauhan U K, Nicols J-Gutierrez, Castineiras A, Magnetic, spectroscopic, structural and biological properties of mixed-ligand complexes of copper(II) with N,N,N',N",N"-pentamethyldiethylenetriamine and polypyridine ligands, *Inorg. Chim. Acta.* 2004;357:2469.
26. Khan M I, Khan A, Hussain I, Khan M A, Gul S, Iqbal M, Rahman I U, Khuda F, Spectral, XRD, SEM and biological properties of new mononuclear Schiff base transition metal complexes, *Inorg. Chem. Commun.* 2013;35;104.
27. Ravi M, Chennam K P, Ushaiah B, Eslavath R K, Perugu S, Ajumeera R, Devi Ch S, A Study on Spectro-Analytical Aspects, DNA – Interaction, Photo-Cleavage, Radical Scavenging, Cytotoxic Activities, Antibacterial and Docking Properties of 3 (1–(6–methoxybenzo[d] thiazol–2–ylimino) ethyl)–6–methyl–3H–pyran-2,4–dione and its Metal Complexes, *J. Fluoresc.* 2015;25:1279.
28. Barton J K, Danishefsky A T, Goldberg J M, Tris(phenanthroline)ruthenium(II): Stereoselectivity in Binding to DNA, *J. Am. Chem. Soc.* 1984;106:2172.
29. Gao F, Chao H, Zhou F, Yuan Y X, Peng B, Ji L N, DNA interactions of a functionalized ruthenium(II) mixed-polypyridyl complex $[Ru(bpy)2ppd]^{2+}$ *J. Inorg. Biochem.* 2006;100:1487.
30. Liu H K, Sadler P J, Metal Complexes as DNA Intercalators, *Acc. Chem. Res.* 2011;44:349.
31. Pyle M A, Rehmann P J, Meshoyrer R, Kumar J N, Turro J N, Barton K J, Mixed-Ligand Complexes of Ruthenium(II): Factors Governing Binding to DNA, *J. Am. Chem. Soc.* 1989;111:3051.

32. Rajarajeswari C, Loganathan R, Palaniandavar M, Suresh E, Riyasdeen A, Akbarsha M A, Copper(II) complexes with 2NO and 3N donor ligands: synthesis, structures and chemical nuclease and anticancer activities, *Dalton Trans.* 2013;42:8347.
33. Ganji N, Chityala V K, Kumar M P, Rambabu A, Vamsikrishna N, Daravath S, Shivaraj, Synthesis, crystal structure and antiproliferative activity of Cu(II) nalidixic acideDACH conjugate: Comparative in vitro DNA/RNA binding profile, cleavage activity and molecular docking studies, *J. Photochem. Photobiol. B.* 2017;175:132.
34. Lakowicz J R, Webber G, Quenching of Fluorescence by Oxygen. A Probe for Structural Fluctuations in Macromolecules, *Biochem.* 1973;12:4161.
35. Suh D, Chaires J B, Criteria for the Mode of Binding of DNA Binding Agents, *Bioorg. Med. Chem.* 1995;3:723.
36. Rambabu A, Kumar M P, Tejaswi S, Vamsikrishna N, Shivaraj, DNA interaction, antimicrobial studies of newly synthesized copper (II) complexes with 2-amino-6-(trifluoromethoxy)benzothiazole Schiff base ligands, *J. Photochem. Photobiol. B.* 2016;165:147.
37. Sigman D S, Nuclease Activity of 1,10-Phenanthroline-Copper Ion *Acc. Chem. Res.* 1986;19:180.
38. Mendu P, Kumari C G, Ragi R, Synthesis, Characterization, DNA Binding, DNA Cleavage and Antimicrobial Studies of Schiff Base Ligand and its Metal Complexes, *J. Fluoresc.* 2015;25:369.
39. Anjaneyula Y, Rao R P, Preparation, Characterization and Antimicrobial Activity studies on some ternary complexes of Cu(II) with Acetyleacetone and various Salicylic Acids, *Synth. React. Inorg. Met-Org. Nano Met. Chem.* 1986;16:257.
40. Tweedy B G, Plant extracts with metal ions as potential antimicrobial agents, *Phytopathology.* 1964;55:910.
41. Sharma A K, Chandra S, Complexation of nitrogen and sulphur donor Schiff's base ligand to Cr(III) and Ni(II) metal ions: Synthesis, spectroscopic and antipathogenic studies, *Spectrochim Acta A.* 2011;78:337.
42. Kumar M P, Tejaswi S, Rambabu A, Kalalbandi V K A, Shivaraj, Synthesis, crystal structure, DNA binding and cleavage studies of copper(II) complexes with isoxazole Schiff bases, *Polyhedron,* 2015;102:111.